Arabian Journal for Science and Engineering
https://doi.org/10.1007/s13369-024-09199-9

RESEARCH ARTICLE-MECHANICAL ENGINEERING

Effect of Number of Channels on Performance of PEM Fuel Cells for Serpentine Type Channel Configuration

Fırat Işıklı[1] · **Hazal Işıklı**[2] · **Ali Sürmen**[1]

Received: 23 January 2024 / Accepted: 16 May 2024
© The Author(s) 2024

Abstract
The number of gas flow channels in a serpentine-type channel configuration for Polymer Electrolyte Membrane Fuel Cells (PEMFC) is a critical design parameter. It influences mass transport, pressure drop, and water management, all of which contribute to the overall performance and efficiency of the fuel cell. In this study, different channel number configurations for small active area fuel cell and their role in contributing to a more sustainable energy environment are discussed. The influence of the number of multiple channels on the operational performance was examined in a fuel cell with 25 cm^2 of active area. Six different flow channel configurations belonging to the traditional serpentine-designed flow channel were utilized, with multiple inlet–outlet structures. Numerical calculations for pressure, velocity, distribution of reactants (oxygen and hydrogen), membrane water content, and changes in water saturation concentration were conducted using the ANSYS Fluent program. The highest power density of 0.657 W/cm^2 was achieved in the single-channel design, resulting in a 14% performance increase compared to the eight-channel design, which exhibited the lowest performance. However, the highest pumping loss due to pressure drop was observed in the serpentine one-channel design at 0.016573 W/cm^2. While the pressure drop enhances performance in the same channel design, when constructing a fuel cell stack with a large number of cells, significant difficulties may arise in procuring a compressor capable of providing the desired pressure and flow rate. Therefore, alternative designs with reduced pressure drop need to be considered.

Keywords PEM fuel cell · Multiple channel · Serpentine channel design · CFD simulation · Channel configuration

1 Introduction

Fuel cells, which are said to operate on the reverse principle of the electrolysis method, were discovered by Sir William Grove in 1839. They produce electricity from chemical energy with a certain efficiency. With the commercialization of these devices for the first time between 1955 and 1958, they have come into the view of energy professionals and continue to be developed day by day [1].

In recent years, rapidly developed fuel cell tech has been seen as a promising solution to the energy problem caused by climate change, air pollution, and scarcity of fossil fuels. PEMFC is preferred in the automotive industry because of its relatively low operating temperature, fast response to variable power demands, and zero emissions [2, 3].

Gas flow channels are one of the most important components affecting the performance [4]. Channel geometry affects the diffusion of gas and liquid, distribution in the active region, chemical reaction rate, current density distribution, and water discharge. Different gas channel designs influence the uniform distribution of reactant gases, under-rib convection intensity, and water removal, thereby determining the performance, service life, and fuel cell energy consumption.

There should be no accumulation of water in flow channels, catalyst layer, and gas diffusion layer (GDL) porous medium. Water (liquid) existence reduces fuel cell performance by blocking reactants reaching the catalyst zone [5, 6]. It should be remembered that chemical reactions occur on the catalyst surface. In effective water management, excess liquid water is drained to the outside, ensuring a sufficient amount of water vapor for proton conduction, while allowing for smooth gas transport without the occurrence of flooding.

✉ Fırat Işıklı
firatisikli@uludag.edu.tr

[1] Department of Automotive Engineering, Bursa Uludag University, Bursa, Turkey

[2] Department of Research and Development, Kırpart Automotive, Bursa, Turkey

Published online: 08 June 2024

To improve performance, different channel geometries, such as parallel [7, 8], serpentine [9–11], interdigitated [12], pin-type [13], and bio-inspired [14–16], have been tested. Among these, the serpentine channel design is often used in the cathode flow channel. Because it is more advantageous in terms of water discharge. The serpentine channel structure within the same active area brings about a higher pressure drop. This condition can reduce the possibility of flooding and at the same time enhance under-rib convection. However, increasing pressure loss requires more power to provide the same flow rate. Consequently, this leads to an increase in parasitic power drawn from the fuel cell.

To reduce pressure drop, designs with multiple serpentine channels are employed. Abdulla et al. examined the effectiveness of an enhanced cross-flow split serpentine flow field (ECFSSFF) design for large reaction zone [17]. They conducted simulations with 50–200 cm^2 active area sizes using a parallel flow design in the anode channel and an improved serpentine design in the cathode channel. Additionally, these designs were compared with fuel cells using a three-channel serpentine bipolar plate on the cathode side. The study indicated that net power output in their developed design increased from 4.5% to 13.5% as the active area grew compared to the triple serpentine design. The change in power density reached levels of 55% with the increase in the active area.

Channel structure effect on PEMFC performance, a comprehensive parametric simulation study was carried out for three-channel conventional and baffled serpentine design [18]. Operating parameter effects such as stoichiometric ratio, temperature, and pressure were also investigated. As long as the values determined for the operating parameter increased, there was an increase in performance for both designs. When baffled flow channel was used instead of the traditional serpentine design, improvements of 16.1% at 1 atm operating pressure, 19.9% at 70°C cell temperature, and 16.1% for a stoichiometric ratio of 2 were achieved. Furthermore, it was noted that when rib/channel width ratio was 1.315 and channel height/width ratio was 1.5 the traditional channel-designed fuel cell exhibited a 53.3% power increase compared to the reference design. The baffled one showed a 58.5% power increase.

Serpentine-designed fuel cell performance was examined through mathematical modeling, considering the gas diffusion layer porosity, channel length, width, depth, temperature, and reactant inlet velocity, [7]. When considering gas, water, and pressure distributions, it was concluded that for the same flow field, an eight-channel serpentine design and an eight-channel complex serpentine design were ideal for cell performance in terms of channel length. It was stated that the eight-channel complex serpentine design provided the best water discharge capability when 1.2 mm width and 0.8 mm depth and the gas distribution was better compared to the others. It was also noted that gas diffusion layer porosity is the main parameter on oxygen, water, and current density distribution.

Wu et al. examined performance characteristics such as membrane water content, proton conductivity, and reactant concentration for 100 cm^2 PEMFC with five different designs: parallel, two- and three-channel serpentine, zigzag, and serpentine-zigzag [19]. The maximum power density for serpentine flow channel designs was 0.33212 W/cm^2 in the serpentine-zigzag flow design, attributed to the equal distribution of reactant and oxidant and effective water discharge. In all configurations, the highest power was obtained at 0.4 V cell voltage. In the two-channel serpentine design, at 100% relative humidity, 0.2639 W/cm^2 power density was achieved, while in the three-channel serpentine design, it increased by 11% to 0.2931 W/cm^2.

It is seen that multi-channel designs are frequently preferred in PEM fuel cells with large active areas [20–22]. It is also a very important issue whether the design effect is in the same direction as the active area becomes smaller. Mojica et al. examined parallel, serpentine, and seven-channel multi-serpentine channel designs to see the effect of channel design on a 5 cm^2 fuel cell [23]. It has been stated that the multi-serpentine design is better at discharging liquid water than the parallel channel design, but is effective up to 80% RH. Although the single-channel serpentine design provides the highest power, it has been observed that the pressure and flow distribution are more balanced in the multi-channel design.

As the fuel cell operates, water is generated on the cathode side. Depending on operating conditions and reaction speed, an increase in the amount of generated water may occur. To ensure continuity of performance, an active drainage channel design method has been proposed in a 25 cm^2 fuel cell [24]. It resembles a multiple channel design in that there are graded interdigitated channels on the right and left sides of the plate and a serpentine channel between them. Although drainage is enhanced with the under-rib convection provided by the design, the power output is close to the serpentine design fuel cell power output. However, when the anode and cathode sides were configured with a serpentine-active drainage design, a 13% increase in power density was observed.

Kaiser et al. examined the effect of channel design on mass transfer in their study on a fuel cell with 25 cm^2 active area [25]. They stated that mass transfer occurs through convection with the wavy channel design. For this reason, they made a performance comparison for the fuel cell with a straight flow channel and multiple wavy channel designs under different stoichiometric operating conditions. As a result of the study, under oxygen excess ratio, $\lambda = 4.8$ conditions, the multiple wavy channel design increased the reactant transfer and also provided an advantage in water discharge.

Boni et al. used three different designs in their experimental study for a 25 cm^2 PEM fuel cell [26]. Two of these designs

have single channels (serpentine and sinusoidal-serpentine), and the other has multiple sinusoidal flow channels. The highest performance was observed in the multi-channel structure fuel cell. At an operating temperature of 60°C, a power density of 0.4232 W/cm^2 was achieved. While the anode humidification temperature was increased to 70°C, the power density reached 0.4608 W/cm^2; the cathode humidification temperature was increased to 70°C, and a power density of 0.5 W/cm^2 was obtained. It has also been stated that as back pressure is increased, although performance increases, pumping loss increases.

The reviewed literature study indicates the beneficial effects of multiple serpentine designs for large and small active areas. For fuel cells with large membrane active areas, multiple serpentine designs are recommended, especially to reduce pumping losses due to high-pressure drops [27].

Active area size, channel design, geometry of channels, and number and orientation of inlets and outlets are important structural issues for typical performance indicators of fuel celle such as pressure drop and power. Since numerous studies show that the dependence of performance on these geometric factors is not systematic, too many analysis combinations need to be tried. Therefore, each analysis carries its own novelty in terms of design-performance relation.

In this context, this study was conducted for 25 cm^2 PEMFC, which is considered small active area. The serpentine design, which is widely used in the literature, was used in a fuel cell with a small active area, and effect of number of multiple input and output channels on the cell performance was examined. The influence of channel numbers on PEMFC performance was examined. For this purpose, 1-2-4-6-8-10 serpentine channel designs were created. Specific channel design dimensions of the fuel cell planned to be produced in the near future were used.

PEM fuel cell analyses were conducted in the ANSYS Fluent environment. Pressure and speed changes within the fuel cell, penetrating reactant concentration distribution to the anode and cathode catalyst, membrane hydration conditions, and liquid saturation changes were examined as possible reasons for the change in cell performance depending on the number of serpentine channels. Moreover, pumping power loss was calculated for each channel design, its effect on net power was investigated and optimal number of channels was determined for 25 cm^2 an active area fuel cell.

2 Material and Method

The purpose of this study is to examine the effects of an increase in the number of channels on the mass transport in a PEM fuel cell with a serpentine channel geometry and an active area of 25 cm^2 under specified operating conditions.

Table 1 Identification of fuel cell components

Components	Assignment	Type
Bipolar plate (anode)	bp_an	Solid
Gas channel (anode)	hydrogen	Fluid
Gas diffusion layer (anode)	gdl_an	Fluid
Catalyst layer (anode)	catalyst_an	Fluid
Membrane	Memb	Fluid
Catalyst layer (cathode)	catalyst_ca	Fluid
Gas diffusion layer (cathode)	gdl_ca	Fluid
Gas channel (cathode)	Air	Fluid
Bipolar plate (cathode)	bp_ca	Solid

This involves investigating the changes in reactant concentration at each channel length, as well as the distribution of pressure, velocity, and water density in the membrane and channels, and evaluating its impact on the performance. The mathematical model was first validated with experimental studies in the literature. Subsequently, as in the model validation stage, a mesh independence study was conducted to run analyses on the 25 cm^2 active area. Calculations were made using ANSYS Fluent computational fluid dynamics software. Calculations were made using the finite volume method with the equations for the transport of gas and liquid phases given in Sect. 2.3.

2.1 Model Verification

The fuel cell analyses were conducted using the ANSYS Fluent 2022 R1 program. In the study, the model was initially validated with previously obtained experimental results in the literature. To do this, the study by [28], commonly used in the literature, was utilized. The design dimensions and boundary conditions for the validation study were implemented based on the values in the relevant study. In the 25 cm^2 active area fuel cell analysis, the design in the reference study was adhered to.

The three-dimensional geometry of the fuel cell used for model validation and all channel configurations was designed in the Solidworks environment and then transferred to the Design Modeler program within ANSYS Workbench. When meshing, all components were consolidated into a single unit using the "Form New Part" command to ensure compatibility of the node points on the contacting surfaces. Subsequently, the flow volume of the bipolar plate, gas diffusion layer, surfaces in contact with the current collector, and the inlet–outlet surfaces of the flow volume were appropriately named.

The fuel cell module constitutes a sandwich structure. The created fuel cell assembly consists of nine-volume regions. Table 1 shows the designations for the components.

Table 2 Quality evaluation of different mesh elements and current density

	Mesh1	Mesh2	Mesh3
Number of elements	18,480	65,100	193,200
Orthogonal quality			
Maximum	1	1	1
Minimum	1	1	1
Skewness			
Maximum	1.8185 e − 010	1.8271 e − 010	1.8271 e − 010
Minimum	1.3057 e − 010	1.3057 e − 010	1.3057 e − 010
Current density	1.143624 A/cm^2	1.149878 A/cm^2	1.150422 A/cm^2

The CAD model that was imported into the ANSYS Workbench environment was divided into finite volumes using the ANSYS Meshing software.

The meshing process is of significant importance for numerical results as it facilitates problem-solving by dividing the flow volumes into smaller segments. Therefore, to ensure the analysis converges accurately and to obtain the most precise solutions, an appropriate numerical mesh structure must be established. The mesh structure of the model is provided in Fig. 3. This study uses a numerical mesh structure consisting of hexahedral (6-faced) elements, as it offers advantages [29].

Chemical reactions take place within the membrane electrode assembly (MEA). For this reason, a mesh structure with more frequent elements in the membrane, catalyst, and gas diffusion layer is preferred. Many model studies in the literature recommend at least four layers of element transitions in these layers [30–32].

Considering this, a mesh structure consisting of 10, 4, and 4 layers for the gas diffusion layer, catalyst, and membrane, respectively, was obtained for all models.

To evaluate mesh quality, "orthogonal quality" and "skewness" values were used as criteria. Criteria related to the number of mesh elements are shown in Table 2. The suitability of the number of mesh elements and mesh density in the model reduces skewness in the mesh structure and improves mesh quality, bringing the analysis closer to real results. In this study, three different mesh structures with varying element counts were created, and it was observed that each mesh had very high quality. The mesh quality and mesh independence results are shown in Table 2. It can be observed that the current density corresponding to 0.6 V does not fluctuate significantly with increases in the number of meshes beyond 65,100.

Table 3 Fuel cell design dimensions with 25 cm^2 active area

Channel width	0.9 mm
Rib width	1 mm
Channel height	0.4 mm
Thickness of catalyst layer [28]	0.0129 mm
Thickness of gas diffusion layer [28]	0.3 mm
Thickness of membrane [28]	0.108 mm
Gas flow channel cross-section	0.4 mm × 0.9 mm

The analysis was performed according to the determined mesh count, and a polarization curve was obtained. A comparison graph with the reference study is provided in Fig. 1. It can be seen that the model is consistent with the referenced experimental study polarization curve. Following the completion of the validation study, the design and analysis process for the fuel cell with a 25 cm^2 active area was initiated.

2.2 Model Development

In the conducted study, following the model validation process, the focus was directed toward the performance effect of different channel numbers for a 25 cm^2 active area. The serpentine design was chosen as the flow channel geometry. This is because the serpentine channel allows for the complete utilization of the active area and facilitates the passage of gas with reasonable pressure losses [33]. Therefore, serpentine designs consisting of single-channel, two-channel, four-channel, six-channel, eight-channel, and ten-channel configurations with the same active area dimensions were employed. Visual representations of flow channel designs are depicted in Fig. 2.

The geometries have a similar pattern, but they possess different channel lengths. As the active area dimension increases, multiple serpentine channels can be preferred [27]. As the number of channels ascends, the number of turns and channel length become less. It has a positive effect on reducing the pressure drop that causes pumping losses. Therefore, the performance effect of multiple channel numbers on the fuel cell with a 25 cm^2 active area has been thoroughly examined. The dimensions of the fuel cell are provided in Table 3. The dimensions provided in the following table were used for all the studies conducted for different channel numbers.

The mesh structure of the fuel cell with a 25 cm^2 active area, divided into finite volumes, is illustrated in Fig. 3. It can be observed that the components of the PEM fuel cell are composed of hexahedral elements, similar to the model validation study. The gas diffusion layer, catalyst layer, and

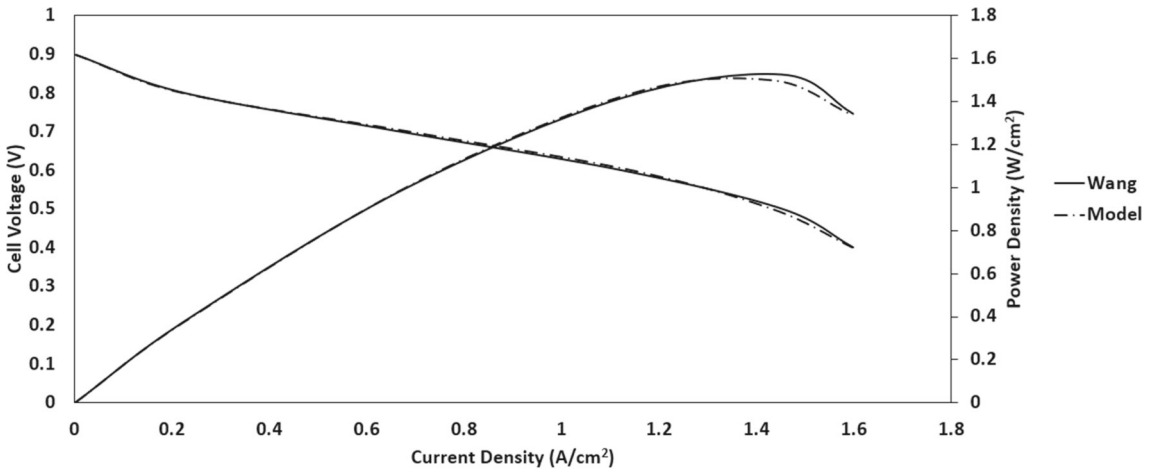


Fig. 1 Polarization curve comparison with Wang model

Table 4 Quality assessment of different mesh elements of the fuel cell with 25 cm^2 active area

	Mesh1	Mesh2	Mesh3
Number of elements	732,608	1,349,560	2,309,872
Orthogonal quality			
Maximum	1	1	1
Minimum	0.87833	0.93445	0.95318
Skewness			
Maximum	0.34205	0.31043	0.21181
Minimum	1.3057 e − 010	1.3057 e − 010	1.3057 e − 010

membrane are constructed with a mesh structure consisting of 10-4-4 layers, respectively.

A mesh independence study was conducted for the single-channel design of the fuel cell with a 25 cm^2 active area. For this purpose, three different mesh element numbers composed of hexahedral elements were used. The mesh element numbers and quality values are provided in Table 4. For computational fluid dynamics analyses, in the model divided into finite volumes, an orthogonal quality of at least ≥ 0.1 and a skewness of at least ≤ 0.9 are generally accepted values. Accordingly, it can be seen that the mesh quality is excellent.

As in the model verification study, a mesh independence study was also conducted for the 25 cm^2 active area fuel cell. Figure 4 shows the variation of current density for three different numbers of mesh elements. When the number of elements exceeded 2 million, the current density converged to a constant value of 1.84 A/cm^2. Considering the computer hardware and solution time, it was deemed impractical to use more than 1.34 million mesh elements for subsequent analyses.

Figure 5 illustrates the power variation with current density and polarization curves for fuel cells with different numbers of channels. In the construction of the curves, analyses were conducted individually for each channel design, starting from a cell voltage of 0.9 V and decreasing in intervals of 0.1 V until reaching a voltage value of 0.3 V, with the current density from the 15000th iteration considered as the steady value and used in the study. When examining the polarization curve, it can be observed that for all channel designs, the fuel cell enters the concentration polarization region at 0.3 V. A lower voltage operating region is not preferable for PEMFC. Therefore, the analyses were conducted based on the lowest cell voltage of 0.3 V.

As the number of channels increases in the fuel cell with a 25 cm^2 active area, the power decreases similarly. However, it should be noted that the power obtained from the 10-channel design is higher than that from the eight-channel design. Therefore, in the following sections, when evaluating the analysis results, the reasons for the performance differences are thoroughly examined based on the results of the 1-8-10 channel designs.

2.3 Setup of the Numerical Model

After the design and meshing processes described in the previous sections, once the model is transferred to the ANSYS Fluent environment, it is necessary to define the boundary conditions and conduct the numerical analysis. In this section, the mathematical equations used in the numerical analysis of the model have been explained [18].

Gas mixture mass conservation equation:

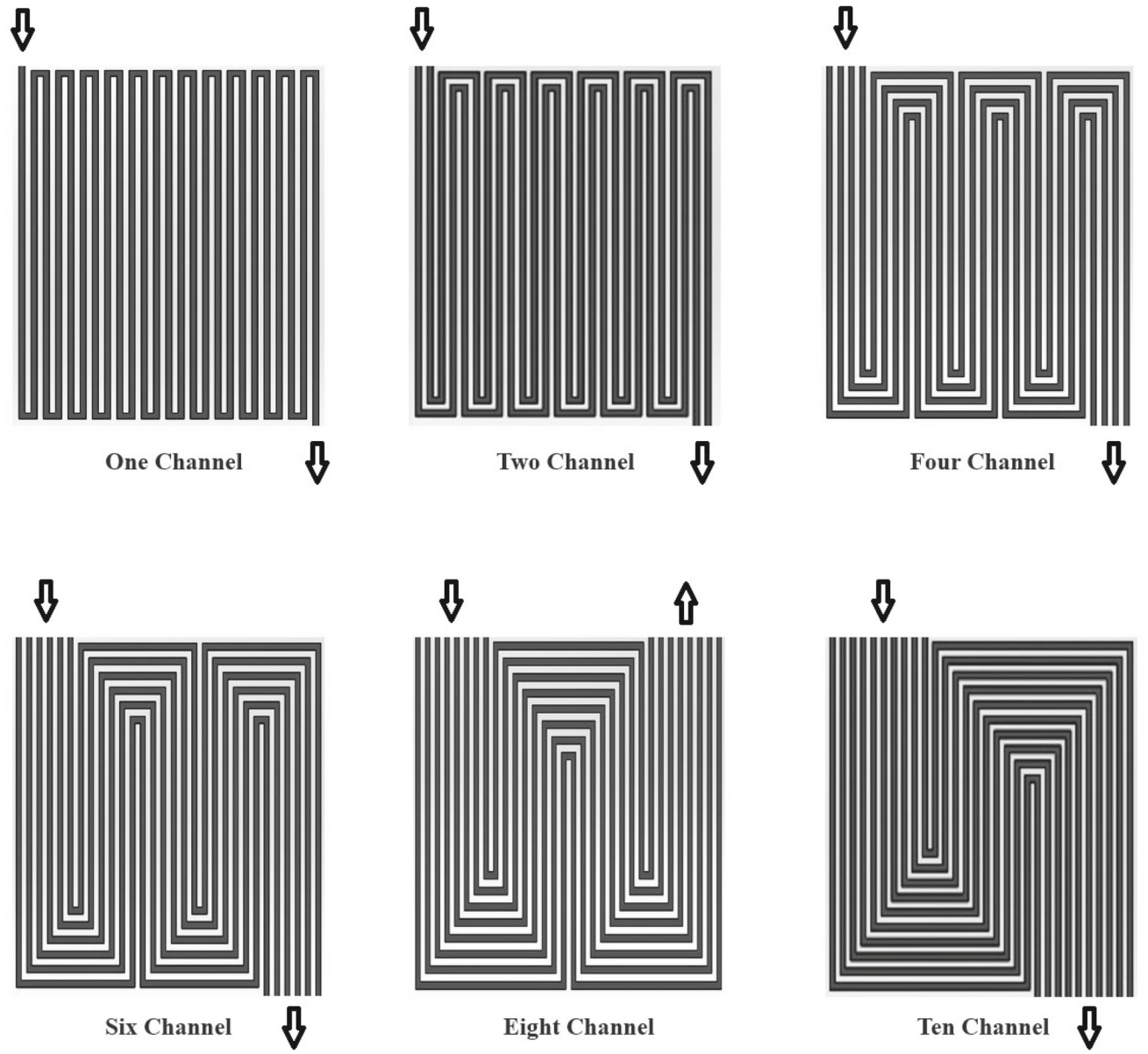


Fig. 2 PEM fuel cell gas flow channels

$$\frac{\partial}{\partial t}\left(\varepsilon\left(1-s\right)\rho_g\right)+\nabla\bullet\left(\rho_g\overrightarrow{u_g}\right)=S_m$$
$$S_m=\sum_k S_k \tag{1}$$

$\overrightarrow{u_g}$, ρ_g is velocity vector and gas mixture density, respectively. ε is porosity. s is water (liquid) saturation.

Gas mixture momentum conservation equation:

$$\frac{\partial}{\partial t}\left(\frac{\rho_g\overrightarrow{u_g}}{\varepsilon\left(1-s\right)}\right)+\nabla\bullet\left(\frac{\rho_g\overrightarrow{u_g}\ \overrightarrow{u_g}}{\varepsilon^2(1-s)^2}\right)$$
$$=-\nabla p_g+\nabla\tau+S_u\qquad S_u=-\frac{\mu_g}{k}\overrightarrow{u_g} \tag{2}$$

p_g is pressure. τ is stress tensor. S_i represents the source term.

Gas mixture species conservation equation:

$$\frac{\partial\left(\left(1-s\right)\rho_g Y_k\right)}{\partial t}+\nabla\bullet\left(\rho_g\overrightarrow{u_g}Y_k\right)$$
$$=\nabla\bullet\left(\rho_g D_k^{eff}\nabla Y_k\right)+S_k\quad k=H_2,\ O_2,\ H_2O,\ N_2$$
$$S_{H_2}=-\frac{M_{H_2}R_a}{2F}$$
$$S_{O_2}=-\frac{M_{O_2}R_c}{4F} \tag{3}$$

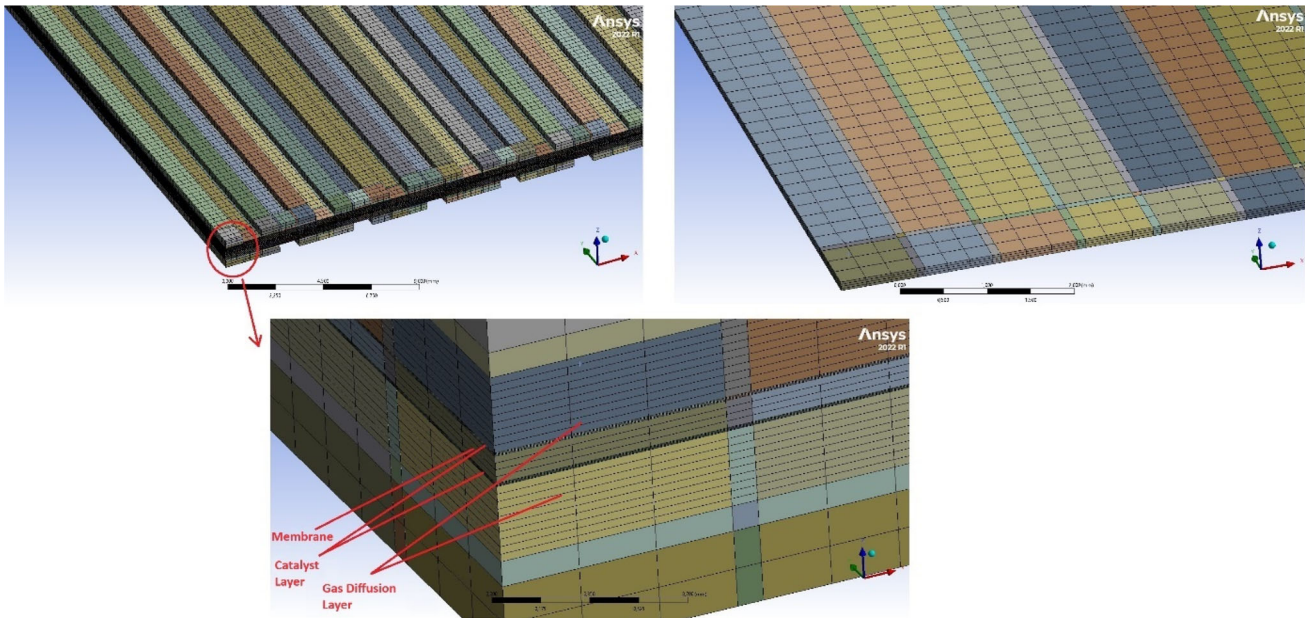


Fig. 3 Single-channel PEM fuel cell network structure with 25 cm^2 active area

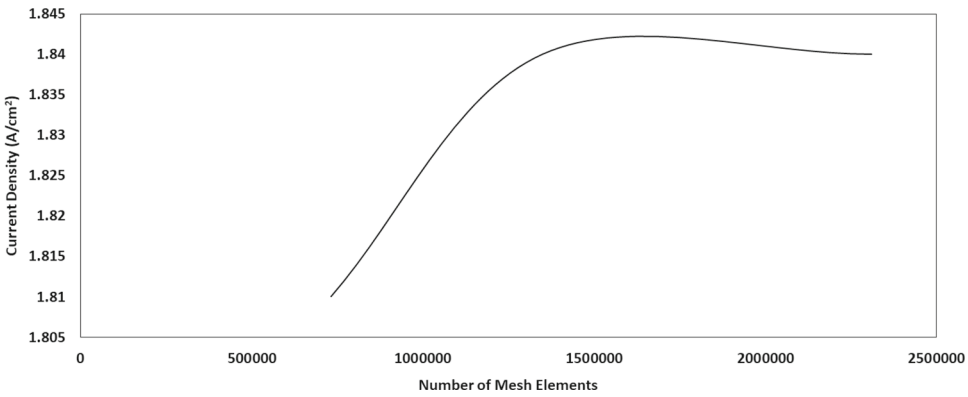


Fig. 4 Mesh independence study for 25 cm^2 fuel cell

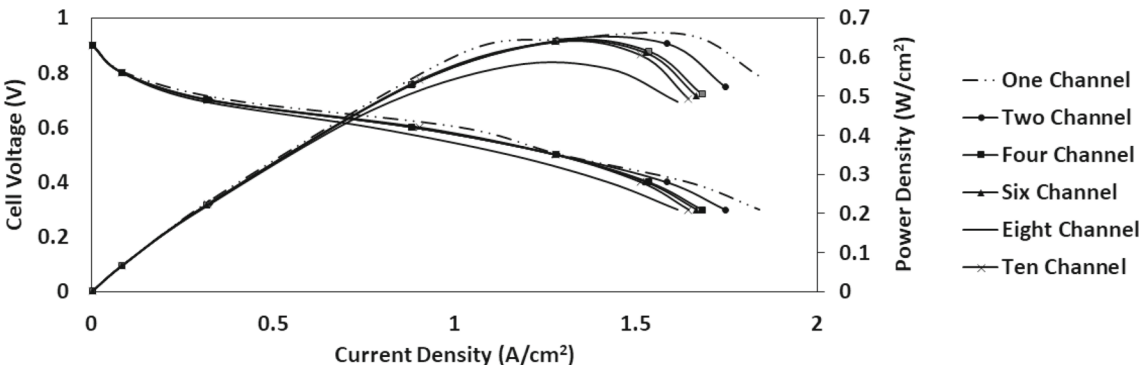


Fig. 5 Polarization curves and power variations of multi-channel fuel cells

Y_k is species mass fraction. D_k is effective coefficient of mass diffusion.

Water dissolved transfer equation in the membrane:

$$\begin{aligned}
&\frac{\partial}{\partial t}\left(\varepsilon_i\, M_{\omega,H_2O}\,\frac{\rho_i}{E\,W}\,\lambda\right)+\nabla\bullet\left(\overrightarrow{i}_m\,\frac{n_d}{F}\,M_\omega\right)\\
&\quad=\nabla\bullet\left(M_\omega\,D_\omega^i\,\nabla\lambda\right)+S_\lambda+S_{gd}+S_{ld}\\
&S_\lambda=-\frac{M_{H_2O}\,R_c}{2\,F}\\
&S_{gd}=(1-s^\theta)\,\gamma_{gd}\,M_{H_2O}\,\frac{\rho_m}{E\,W}\,(\lambda_{\text{equil}}-\lambda)\\
&S_{ld}=s^\theta\,\gamma_{ld}\,M_{H_2O}\,\frac{\rho_m}{E\,W}\,(\lambda_{\text{equil}}-\lambda)
\end{aligned}\tag{4}$$

ε_i is the volumetric fraction of the polymer membrane. $\overrightarrow{i}_m$ is the ion current density. λ is water content in membrane. n_d is the electrostatic resistance coefficient. D_ω^i is water diffusion coefficient. ρ_i is density of the polymer membrane, and $E\,W$ is equivalent molecular weight of the membrane.

Liquid water mass conservation equation:

$$\begin{aligned}
&\frac{\partial}{\partial t}\left(\varepsilon_i\,\rho_l\,s\right)+\nabla\bullet\left(\rho_l-\frac{K\,k_{rl}}{\mu_l}\,\frac{\mathrm{d}p_c}{\mathrm{d}s}\,\nabla_s\right)\\
&\quad+\nabla\bullet\left(\frac{\mu_g\,k_{rl}}{\mu_l\,k_{rg}}\,\rho_l\,\overrightarrow{u_g}\right)=S_{gl}-S_d\\
&S_{gl}=\begin{cases}\dfrac{\gamma_e\,\varepsilon\,s\,D_{gl}\,M_{H_2O}}{R\,T}\,p\,\ln\left(\dfrac{p-p_{sat}}{p-p_{wv}}\right) & if\ p_{wv}\le p_{sat}\\[2ex] \dfrac{\gamma_c\,\varepsilon\,(1-s)\,D_{gl}\,M_{H_2O}}{R\,T}\,p\,\ln\left(\dfrac{p-p_{sat}}{p-p_{wv}}\right) & if\ p_{wv}>p_{sat}\end{cases}
\end{aligned}\tag{5}$$

ρ_l is liquid water density. μ_i is dynamic viscosity. K is porous material permeability, k_i is relative permeability.

Electronic and protonic charge conservation equation:

$$\begin{cases}\nabla\bullet\left(-\sigma_s^{eff}\,\nabla\varphi_s\right)=R\\ \nabla\bullet\left(-\sigma_m^{eff}\,\nabla\varphi_m\right)=-R\end{cases}\tag{6}$$

R is the volumetric current density. σ_s^{eff} is solid material electric conductivity. And σ_m^{eff} is polymer membrane electrical conductivity. φ_s and φ_m are electric potential.

A humidified hydrogen stream enters the fuel cell through the anode inlet channel. There is no liquid fluid entering the channel. Humidified air flow enters the fuel cell through the cathode inlet channel. Here too, there is no liquid fluid entering the channel. Boundary conditions used in the model are given in Table 5. Except for the shared boundary conditions, they were used as default values assigned by the program.

The fundamental assumptions made in the current study are as follows:

- Flow of chemical components (H_2, O_2, H_2O) and liquid water transport are considered laminar.
- Formation of liquid water and transport are included in the numerical solution.
- The analysis is performed for steady-state conditions.
- MEA materials are assumed to be isotropic.
- All gases are considered as ideal gases.

Table 5 Boundary conditions of a 25 cm^2 fuel cell

Anode flow rate (kg/s)	5.469×10^{-7}	Cathode flow rate (kg/s)	1.8726×10^{-5}
Anode temperature (K)	343.15	Cathode temperature (K)	343.15
Anode relative humidity	50%	Cathode relative humidity	50%
Anode stoichiometric ratio	1.2	Cathode stoichiometric ratio	2
Anode pressure (Pa)	200 000	Cathode pressure (Pa)	200 000
Hydrogen mass fraction	0.568446	Oxygen mass fraction	0.2213558
Anode inlet water mass fraction	0.431554	Cathode inlet water mass fraction	0.05001469

In the analysis, a Dell Precision 5820 Tower computer with an Intel(R) Xenon(R) W-2155 processor and 32 GB RAM was used. The solution was performed with a 10-core parallel processor in the Fluent program. Laminar flow occurs within the fuel cell. The solution time for each cell voltage was 15 h. The solution for each design occupies 8–10 GB of memory space.

During the calculations, to manage the pressure–velocity coupling in the gas mixture, the SIMPLE (Semi Implicit Method for Pressure Linked Equations) algorithm, commonly preferred in fuel cell analyses [34, 35], was used. Furthermore, for fuel cell analysis, the first-order upwind spatial discretization was preferred for the transport equations of species (defined as H_2, O_2, H_2O in Fluent) and momentum due to its ease of convergence. The energy convergence criterion was determined as $1e^{-6}$, and the other convergence criteria were determined as $1e^{-3}$. Convergence criteria was achieved in the analysis.

3 Results and Discussion

In this section, the numerical results of the serpentine design comprising 1-8-10 channels 25 cm^2 active area under the same operating conditions fuel cell were evaluated. Figure 5 presents the polarization curves and power density graphs for all channel designs. Upon examining the performance characteristics of these three designs, it is evident that the

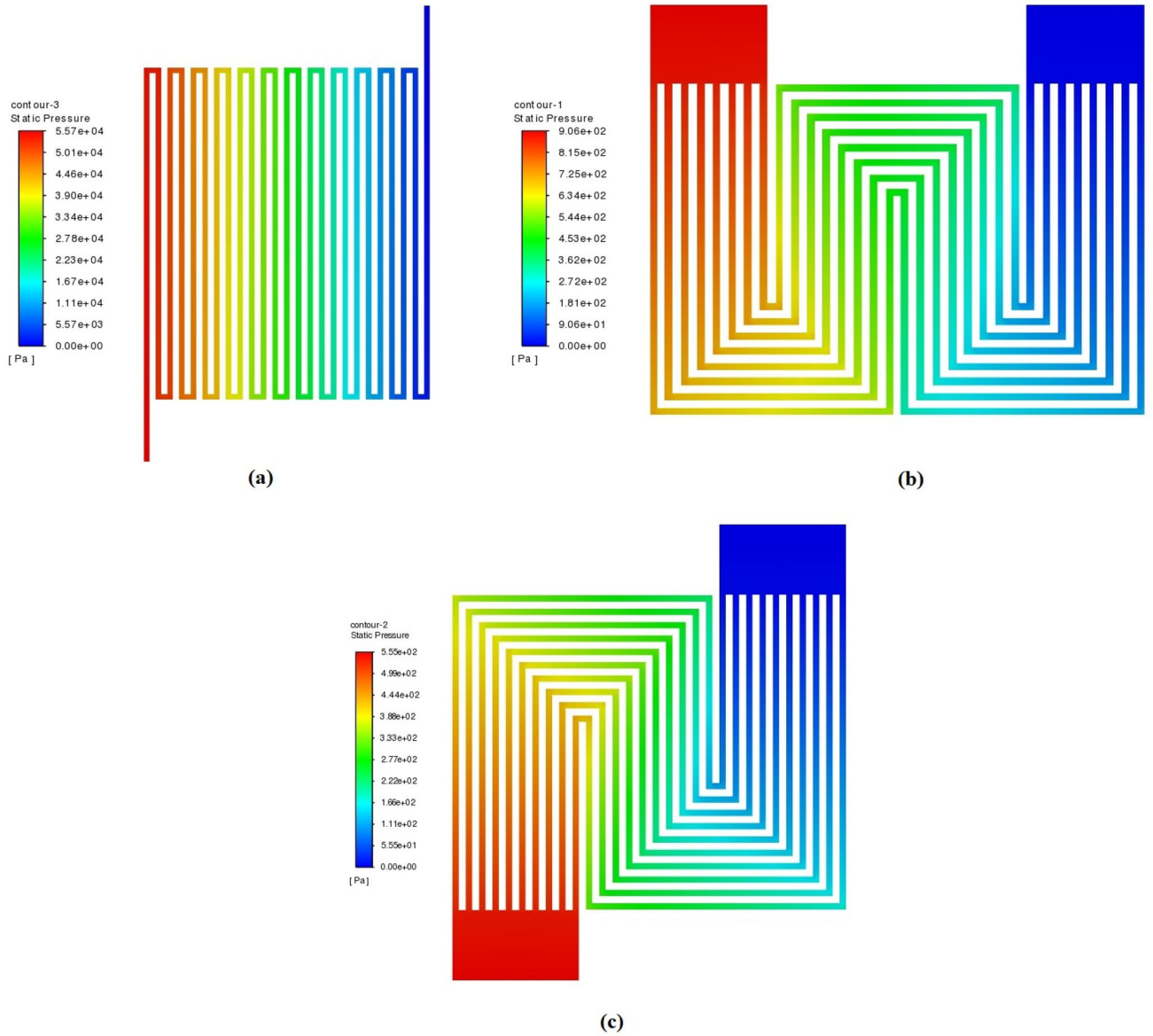


Fig. 6 **a** Cathode channel pressure distribution of the single-channel fuel cell, **b** the eight-channel fuel cell, and **c** the ten-channel fuel cell

single-channel design with a power density of 0.657 W/cm^2 outperforms the other two designs with a maximum power increase of approximately 14%. The power densities of the eight-channel and ten-channel designs are 0.575 W/cm^2 and 0.639 W/cm^2, respectively. The performance decreases as the number of channels increases for the same active area. Several potential factors contribute to this phenomenon, one of which is pressure drop. The following figures utilize visuals corresponding to the operating conditions that yield the highest power when evaluating performance. Figure 6 shows the pressure distribution of different cathode channel designs.

In all three designs, there is high pressure in the initial inlet channels. Along the MEA, the pressure gradually decreases as the reactant gases are depleted in the channels. Fuel cell overall performance and mass transport are managed based on this characteristic. The inlet–outlet pressure differences were 55,693.5 Pa for the single channel, 905.233 Pa for the eight-channel, and 554.377 Pa for the ten-channel design. Accordingly, the highest pressure drop was observed in the single-channel design.

This situation can be interpreted as follows: It is known that the cathode channel exhausts the fluid to the atmosphere. For the fluid entering the channel to continue its flow without losses, the inlet of the channel with high-pressure drop needs to have relatively higher pressure. Therefore, more reactions occur in regions where the pressure is higher compared to the other examined channels. The performance curve given

in Fig. 5 shows that the single-channel design provides the highest power.

Pressure drop is critical for the evaluation of the fuel cell system, as it is directly related to the pumping power that supplies fuel/oxidant to the fuel cell. As the pressure drop increases, pumping losses also increase, leading to a rise in the parasitic power drawn from the fuel cell. First and foremost, it should be understood that reducing the pressure drop within the channel is beneficial for enhancing fuel cell performance, but it is not the only factor affecting performance. Therefore, reducing pressure drop does not necessarily mean achieving the best performance.

Plates with poor design may not perform adequate water drainage, hindering the reactant transport. Furthermore, channel design can cause non-homogeneous reactant distribution, affecting the catalyst layer's utilization [36]. However, high-pressure loss may affect the penetration of more reactants to the catalyst surface [37]. Additionally, high-pressure drop increases the forced transport of liquid water, facilitating its removal. On the other hand, it also increases the power loss required by the compressor. Therefore, the optimum level of pressure drop should be determined.

In Fig. 7, velocity variations in the cathode channel with three different flow channel designs are depicted. Variations in fluid velocity are observed due to changes in pressure within the channels. In the single-channel design, which experiences the highest pressure drop, it is evident from the velocity distribution that the velocity increases in the exit regions where the pressure drop is the most significant. In this region, the fluid reaches a maximum velocity of 28.7 m/s, which is the highest among the analyzed flow channel designs. The average velocity in the cathode channels is 18.3 m/s. The maximum velocities in the eight-channel and ten-channel designs are 5.63 m/s and 3.74 m/s, respectively, with average velocities of 3.039 m/s and 2.35 m/s.

When examining fluid velocities in the eight-channel and ten-channel fuel cells, it is evident that the ten-channel design achieves a lower velocity. This condition positively influences the residence time of the reactant (oxygen) inside the channels, allowing it to diffuse to the catalyst surface and participate in the reaction. It is known that the single-channel design has the longest length, and increasing the number of channels reduces the length to mitigate pressure losses. Based on this assessment, it can be concluded that in the ten-channel design, the lower average fluid velocity inside the channels has a positive effect on fuel cell performance.

Furthermore, it is easy to observe boundary layers along the channel walls. Water typically accumulates near the walls, creating a circular gas flow [33]. The blue areas in the velocity contour images in Fig. 7 likely indicate dead zones. These zones suggest that the reactant gas does not come into contact with the membrane/catalyst surface. Structural modifications are required to address these regions.

If we need to summarize the results regarding pressure and velocity: As the channel numbers ascend, pressure drop becomes less. With the increase in the number of channels, the pressure distribution begins to homogenize, resulting in an increase in the average pressure compared to the inlet air pressure and a decrease in the average velocity. When evaluating the above pressure and velocity graphs, it can be observed that the low reactant velocity in fuel cells with small active areas (e.g., 5 cm^2, 25 cm^2) contributes positively to the chemical reaction by allowing the reactant to stay in the active area for a longer period. However, in the single-channel design, the length of the channel is not the same as that of each channel in the multiple-flow channels. Therefore, we cannot simply say that the increase in velocity in the single-channel design alone reduces the performance. Additionally, when looking at Fig. 8, it can be seen that all of the hydrogen are completely consumed at the channel outlet. Thus, it is possible to say that the reactant remains inside for a sufficient duration.

Another parameter affecting fuel cell performance is the quantity of reactant penetrating the catalyst surfaces. As the reactant concentration of the catalyst surface increases, getting into the concentration polarization region is delayed. This is possible when the pressure drop is low and the reactant is uniformly distributed throughout the flow channel [37]. High-pressure drop causes rapid local reactions and negatively affects fuel cell performance due to inadequate regional fuel/oxidant supply.

In Figs. 8, 9, and 10, the mass fraction ratios of the reactants under the highest power conditions for the three different fuel cells were obtained for both the anode and cathode sides. These values essentially indicate the reactant concentration within the fluid. The image at the top represents the concentration distribution of the reactant on the cathode side for each fuel cell design, and the image at the bottom represents the concentration distribution of the reactant on the anode side.

Oxygen concentration directly affects the electrochemical reaction rate. In all analyses, the oxygen concentration entering the fuel cell was stated as 0.2213558 in the boundary conditions table. When looking at Fig. 8, it can be seen that the maximum oxygen concentration diffused to the cathode catalyst/GDL surface is 0.210. The oxygen concentration is high in the first half of the interface. However, cathode channel oxygen concentration gradually diminishes, resulting in less oxygen remaining for the downstream regions of the active surface (catalyst/GDL surface). Consequently, the oxygen concentration on the active surface decreases significantly to 3.22×10^{-5}.

A similar change is observed for hydrogen on the anode side. However, it is observed that all of the hydrogen reacts throughout the active area surface, and therefore, no hydrogen is found at the anode channel outlet. In the reactant

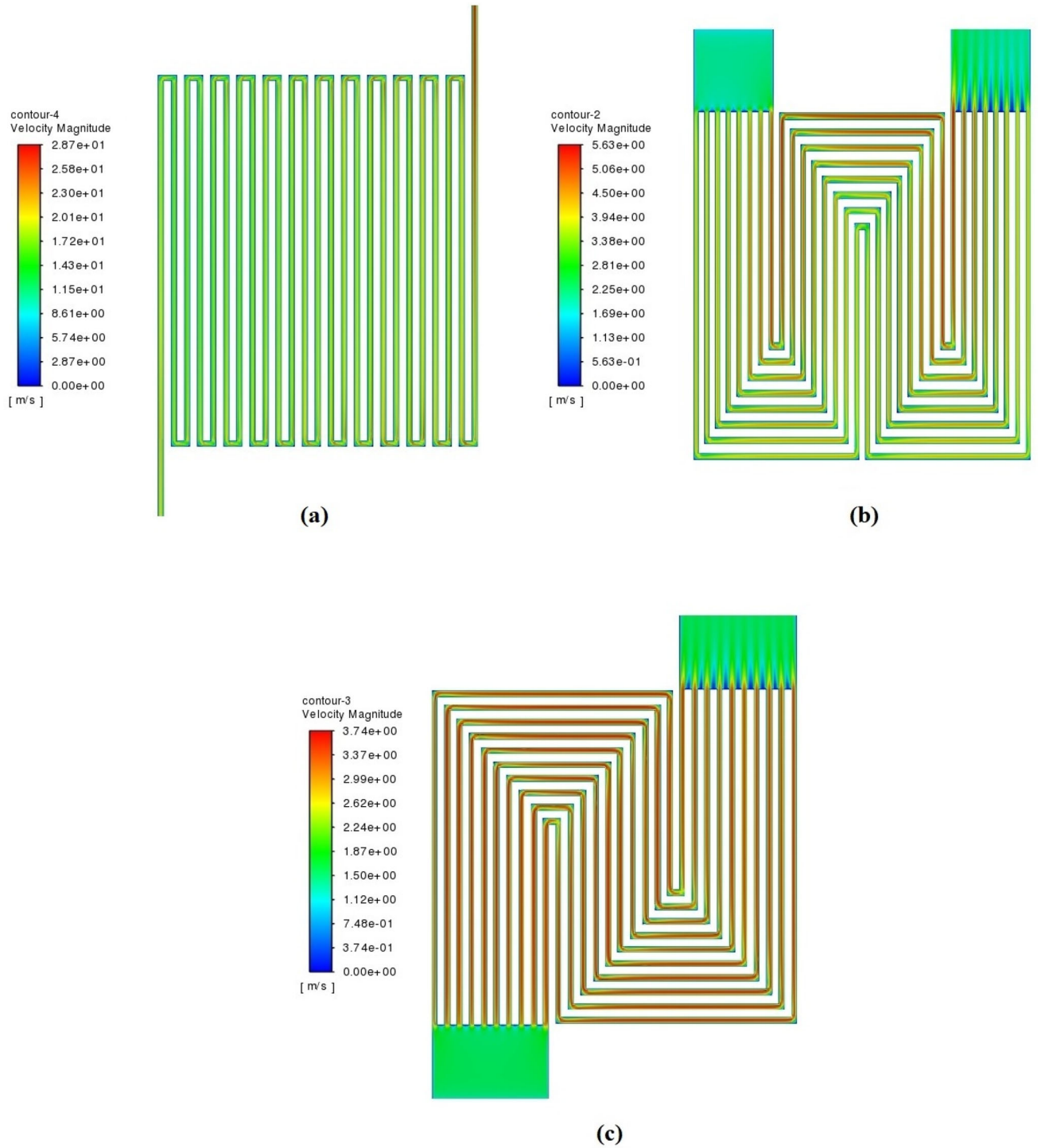


Fig. 7 **a** Velocity distribution in single-channel, **b** eight-channel, and **c** ten-channel fuel cell cathode channels

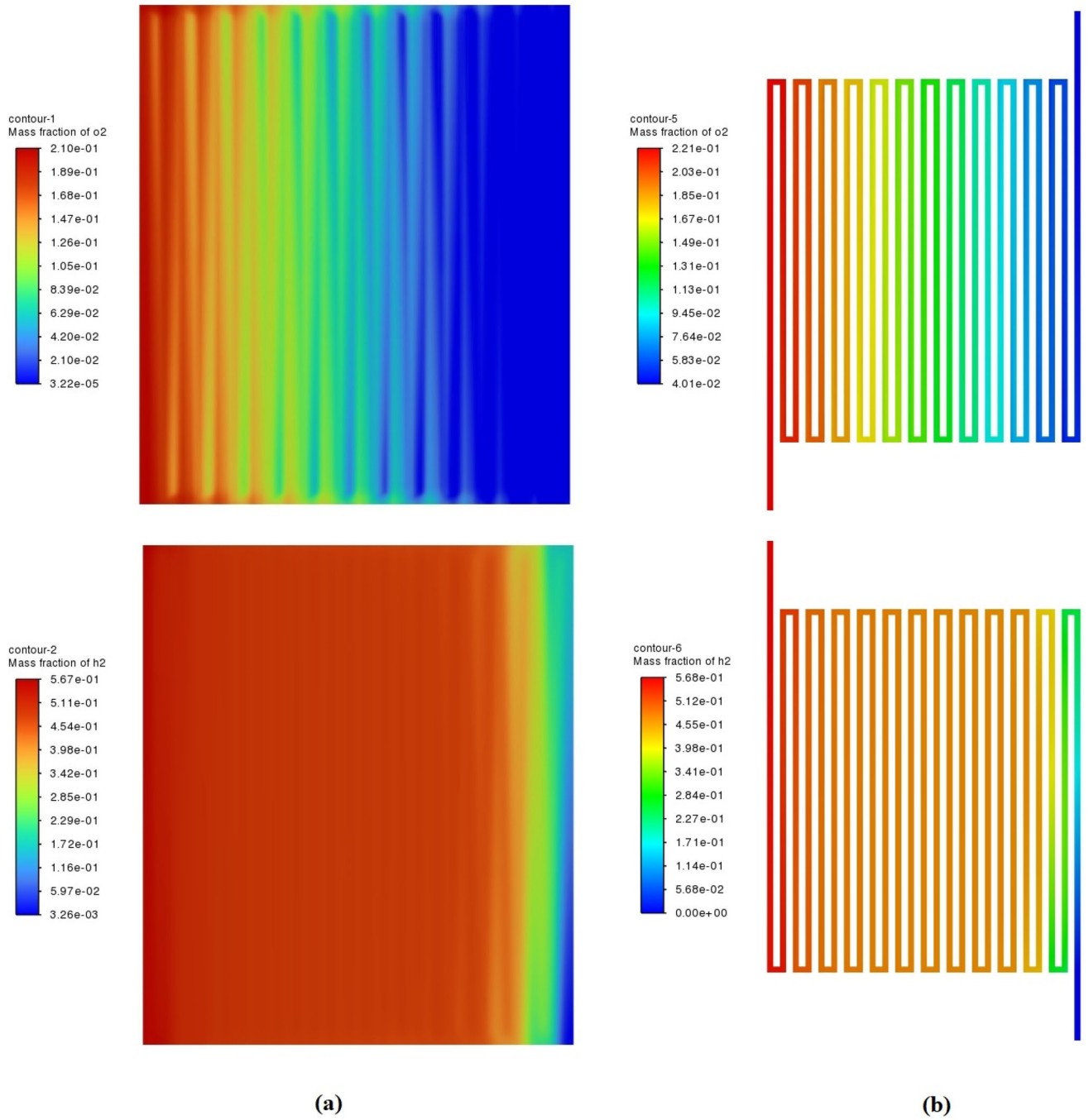


Fig. 8 Oxygen and hydrogen concentration distributions on the **a** catalyst/GDL surface and **b** in channels of the single-channel fuel cell

concentration distribution on the anode and cathode catalyst surfaces, the blue areas indicate oxygen- and hydrogen-depleted regions. To achieve higher power from the fuel cell, more reactants should penetrate these dead regions within the active area.

In Fig. 9, when looking at the contours of the eight-channel fuel cell, the distributions of reactants on the catalyst/GDL surfaces and in the channels exhibit parallelism. For the cathode side, in the inlet region, the maximum oxygen concentration on the catalyst surface is 0.211, while the average oxygen concentration is at the 0.1 level. On the anode side, the maximum hydrogen concentration penetrating the catalyst is 0.57, and the average hydrogen concentration is 0.44. These values are higher than those in single channel. However, it is observed that more reactants (both oxygen and hydrogen) are leaving the fuel cell without being used at the channel

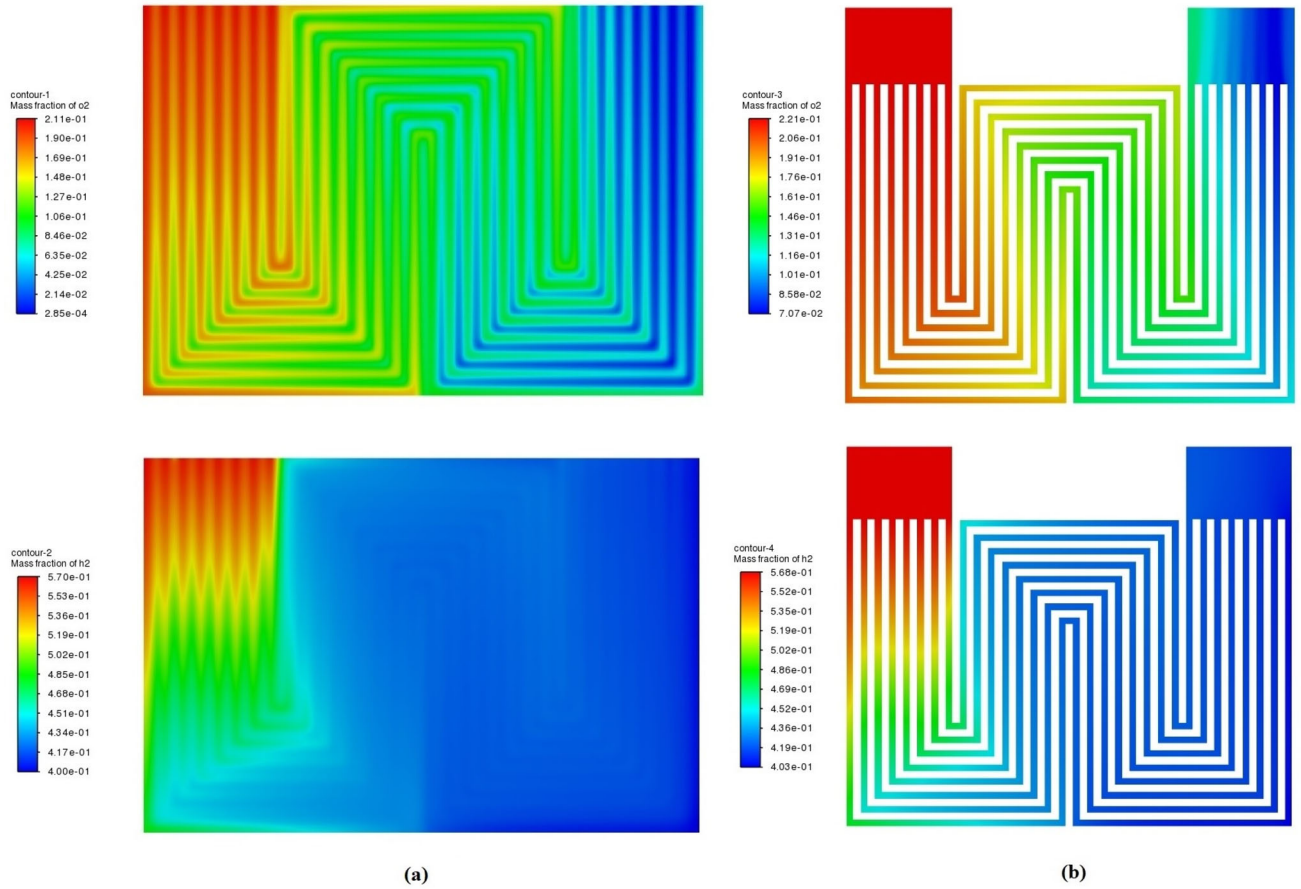


Fig. 9 Concentration distribution of oxygen and hydrogen on the **a** catalyst/GDL surface and **b** in channels of the eight-channel fuel cell

outlets. In comparison with the single-channel fuel cell, at the anode channel outlet, some hydrogen is seen leaving the fuel cell without reacting. This is directly indicative of the channel pressure difference, resulting in the lowest power output among the three designs under consideration.

When looking at the concentrations of oxygen and hydrogen in Fig. 10, the highest reactant concentration values at the channel inlet are 0.552 for the anode and 0.207 for the cathode catalyst/GDL surfaces. These values indicate that the lowest concentration is achieved in the ten-channel fuel cell design. The average mass fractions of reactants on the anode and cathode sides are 0.46 and 0.08, respectively. However, unlike the eight-channel design, it is important to note that all the hydrogens entering the fuel cell are utilized.

Membrane hydration is also important for the fuel cell. Uniform water distribution in the membrane (without flooding) is a method used to extend the life of the PEM fuel cell. This is because localized hotspots and flooding can stress the membrane, potentially causing damage [38].

In Fig. 11, average membrane hydration values for three different fuel cell designs are provided. It is seen that as the current density rises, the membrane hydration increases. This is because at higher current loads, more water is generated due to the chemical reaction. Increased membrane hydration has a positive effect on proton conductivity, contributing to the rise of overall performance. The relatively low membrane hydration in the eight-channel design is among the possible reasons for achieving the lowest power output.

The analysis results show that there is a change in the operating performance as the channel count increases in the 25 cm^2 active area fuel cell. One of the parameters affecting the result is liquid saturation. Low liquid water content reduces mass transfer losses and improves fuel cell performance.

More explicitly, the water production rate is related to the current production. High current densities result in high water production. Therefore, at high currents, mass transfer losses become dominant in the fuel cell. Liquid water reduces PEM fuel cell performance as follows:

- By obstructing catalyst and GDL porosity, reducing the concentrations of gases (hydrogen and oxygen) on catalyst surface,

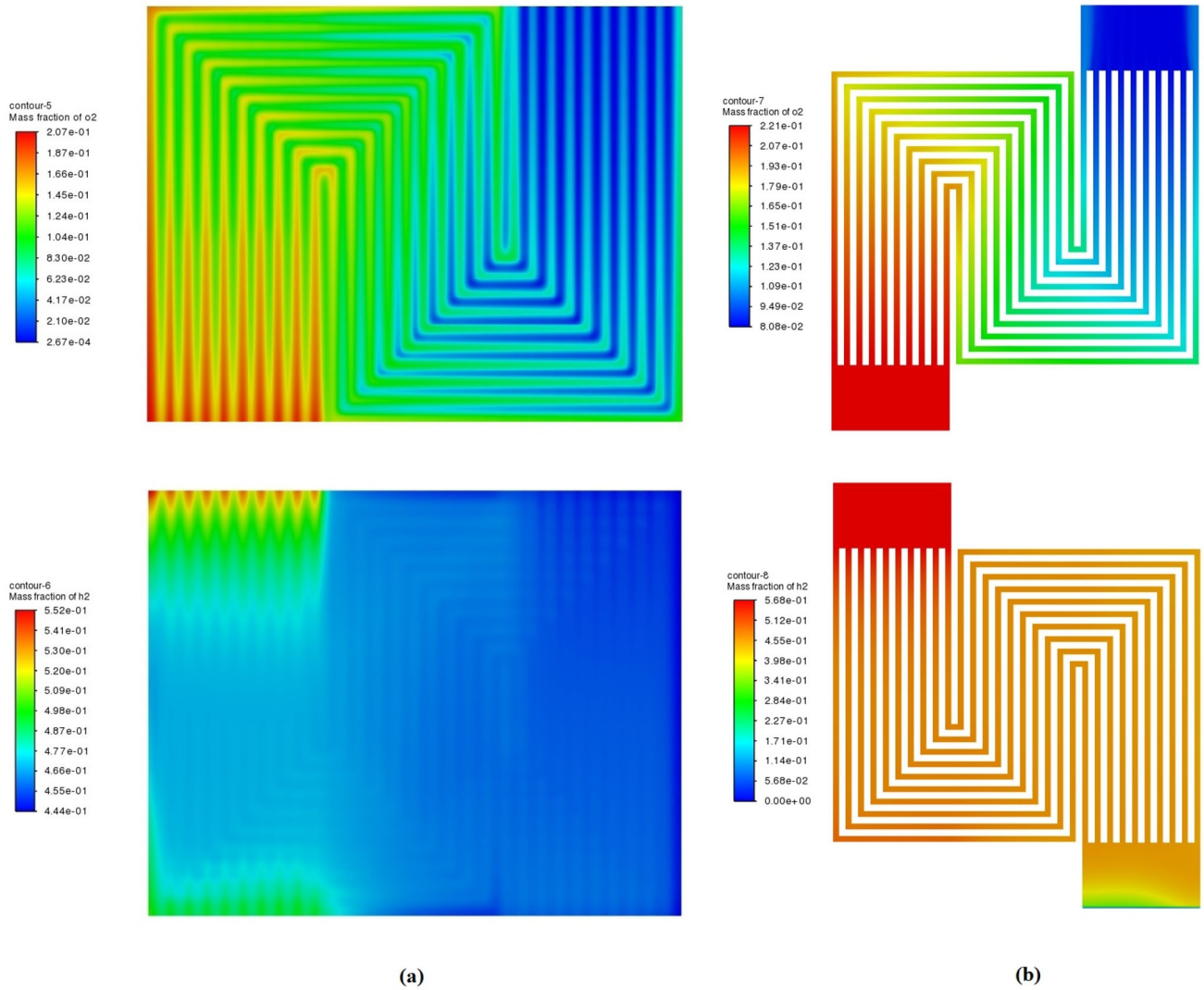


Fig. 10 Concentration distributions of oxygen and hydrogen in the **a** catalyst/GDL surface and **b** in channels of the ten-channel fuel cell

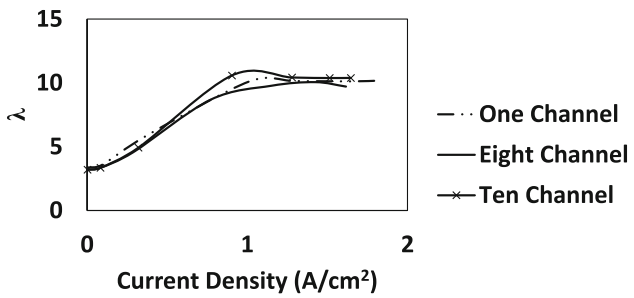


Fig. 11 Membrane hydration (λ)

- By covering catalyst layer active area with water, it is prevented the electrochemical reaction from taking place. From this perspective, the calculation equation for gas diffusion is provided in Eq. (7). The term "s" used in the equation represents the water saturation that leads to performance degradation due to pore blockage.

$$D_i = \varepsilon^{1,5}(1-s)^{r_s} D_i^0 \left(\frac{P_0}{P}\right)^{\gamma_p} \left(\frac{T}{T_0}\right)^{\gamma_t} \quad (7)$$

In the simulation, the cathode channel and the GDL interface were examined to observe this effect. According to the polarization curve, it can be seen that concentration losses become more pronounced during operation below 0.4 V of cell voltage. Therefore, in Fig. 12, the changes in liquid saturation at the cathode flow channel and GDL interface are shared for the three different fuel cells corresponding to the current conditions at 0.4 V of cell voltage.

When looking at the maximum saturation, the lowest saturation is observed to be 0.151 in the 10-channel design. The maximum saturation in the other two designs is in the

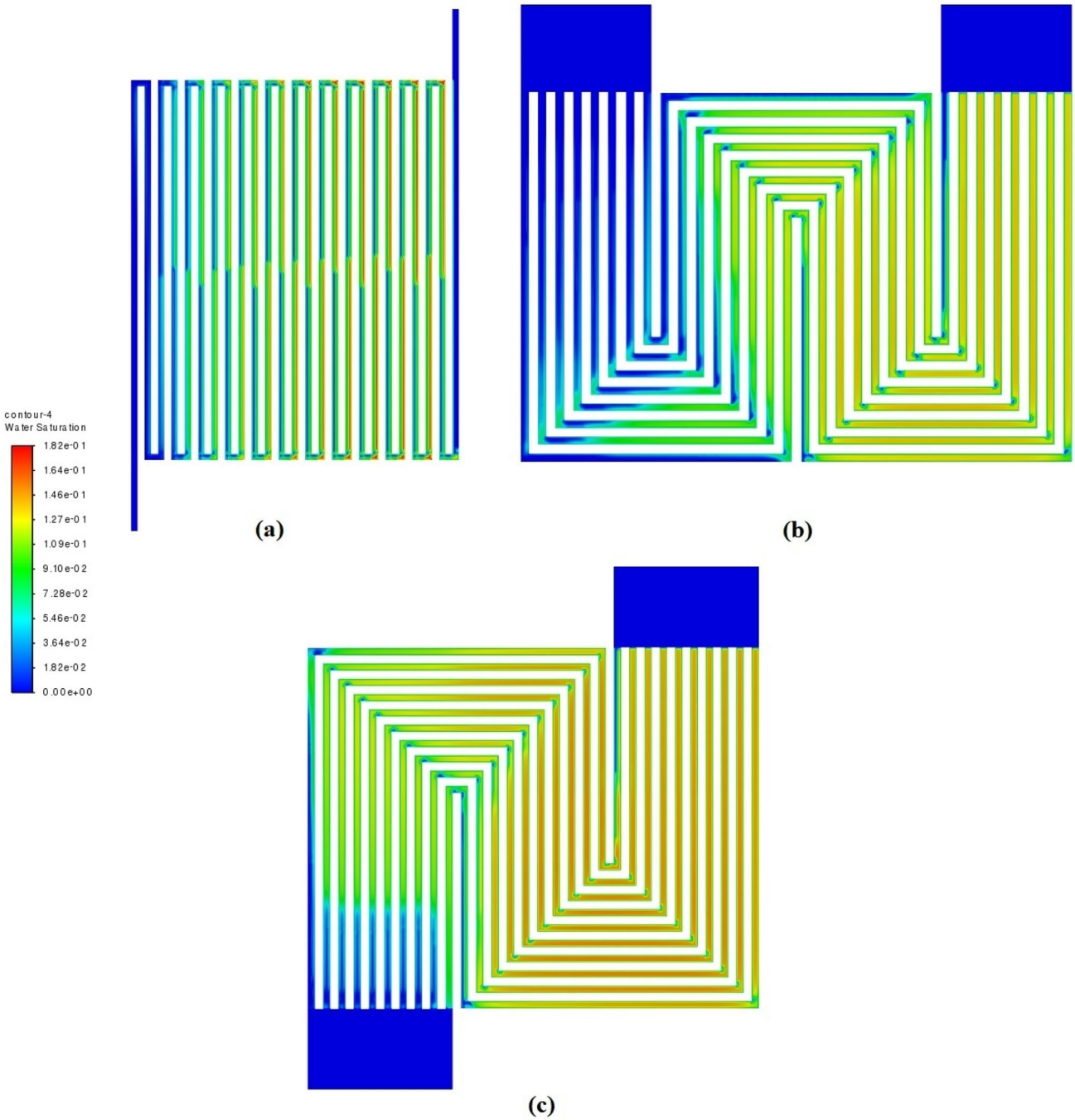


Fig. 12 **a** single-channel, **b** eight-channel, and **c** ten-channel fuel cell cathode channel/GDL water saturation

order of 0.18. The ten-channel design performs better than the eight-channel design, reducing mass transfer losses and increasing fuel cell performance.

Table 6 shows the total pressure drop, pumping losses, and net power changes of the three channels examined according to their operating voltages. While high-pressure drop improves fuel cell performance, it also implies the need for more power for the compressor to provide sufficient airflow to the cathode channel. This will lead to a decrease in the net power obtained from the fuel cell. The relationship between the pressure drop in the channels and the pumping losses is provided by Eq. (8).

$$W_p = \frac{\Delta P_{\text{tot}} A_{ch} \upsilon}{A_{\text{tot}}} \tag{8}$$

Table 6 Pumping losses of 1-8-10 channel designs for 25 cm^2 active area

Number of channels	Voltage (V)	ΔP (Pa)	W_loss (W/cm^2)	W_net (W/cm^2)
One channel	0.7	57,277.88	0.0169548	0.248892
	0.6	56,902.86	0.0168718	0.591794
	0.5	56,350.28	0.0167460	0.629897
	0.4	55,594.00	0.0165730	0.641362
	0.3	54,935.14	0.0164217	0.535871
Eight channel	0.7	901.09	0.0000217	0.201549
	0.6	908.47	0.0000219	0.462001
	0.5	904.48	0.0000218	0.575721
	0.4	901.29	0.0000217	0.569647
	0.3	902.43	0.0000217	0.484830
Ten channel	0.7	563.81	0.0000107	0.224528
	0.6	563.13	0.0000107	0.542209
	0.5	553.97	0.0000105	0.639633
	0.4	547.36	0.0000104	0.605680
	0.3	543.33	0.0000103	0.493881

In the equation, W_p the loss power density is expressed in terms of ΔP_{tot} the total pressure drop, A_{ch} the cross-sectional area of the flow inlet, A_{tot} the total reaction area, and υ the gas inlet velocity on the cathode side. When looking at the table, it can be observed that the pressure drop amounts vary for the different cell voltages. As the channel numbers change, the pressure drop changes dramatically. However, the same channel design does not yield the same effect as the voltage changes concerning the pressure drop. Since the highest pressure drop is in the single-channel design, the highest pumping loss occurs in this design. The calculated pumping losses for the operating conditions where the highest power is obtained are as follows: 0.016573 W/cm^2 for the single-channel design, 0.0000217 W/cm^2 for the eight-channel design, and 0.0000105 W/cm^2 for the ten-channel design. It should be noted that the calculated values are for a single-cell fuel cell. It is a known fact that for multicell stack, the required pressure and compressor power will be much higher. Moreover, the difficulties that may arise in providing the necessary compressor power for large-area fuel cells should not be ignored, as they may eliminate the performance advantage of pressure drop.

4 Conclusion

Small active area PEMFC performance analyses were examined. The influence of bipolar plate multi-serpentine flow channels on local pressure distribution, oxygen concentration, hydrogen concentration, water concentration, membrane water content, and flow velocities of the fluids in the channels on the system's performance was investigated. Additionally, pumping losses resulting from pressure drop were calculated, and the impact of the power losses spent on the compressor on the net power was evaluated. The results are summarized as follows:

- The high-pressure drop can facilitate reactant diffusion and contribute to liquid water discharge, but it also reduces net power by increasing pumping losses. Under the conditions where the highest power was achieved, the total pressure was 55,594 Pa for the single-channel design, 901.29 Pa for the eight-channel design, and 553.97 Pa for the ten-channel design. Thus, the highest pressure drop was observed in the single-channel design.
- Flow velocity increased at the outlet regions where pressure loss was most significant within the flow channels. The single-channel design with the highest pressure drop exhibited a maximum velocity of 28.7 m/s in the cathode channel, which was the highest velocity among the examined designs. Multi-serpentine channels lead to lower flow velocity. However, the ten-channel design had a lower velocity than the eight-channel design, which positively affected the residence time of reactants inside the channels.
- The oxygen and hydrogen concentrations penetrating the catalyst layer directly influence the electrochemical reaction rate. In all designs, the high oxygen concentration at the inlet decreased toward the outlet as it reacted. This decrease was consistent with the change in reactants along the channels. Single-channel design consumed the most oxygen, reducing its mass fraction to 3.22×10^{-5}.
- Similar effects were observed on the anode side for hydrogen. However, in the single-channel and ten-channel

designs, all the hydrogen participated in the reaction. In the eight-channel design, hydrogen was expelled from the channels without using all of it. For this reason, the power output was the lowest.

- With higher loads, the membrane water content increased due to the reaction rate. The eight-channel design had the lowest membrane water content for all current loads. In all designs, the water did not reach saturation or change to the liquid phase. Therefore, the eight-channel design, where water content that enhances proton conductivity was the lowest, achieved the lowest power.
- When examining pumping losses, it was observed that pressure drop and pumping losses were not affected by changes in cell voltage for the same design. However, an increase in the number of channels affected both of these factors. Choosing a single-channel serpentine design over the ten-channel design increased pumping losses from 0.0000105 W/cm^2 to 0.016573 W/cm^2. It should be noted that this value is for a single cell, and it is evident that for a stack comprising multiple cells, the required pressure and compressor power will be much higher, especially for large-area fuel cells like 200 cm^2. Therefore, determining the optimum point is crucial.

Funding Open access funding provided by the Scientific and Technological Research Council of Türkiye (TÜBİTAK).

Open Access This article is licensed under a Creative Commons Attribution 4.0 International License, which permits use, sharing, adaptation, distribution and reproduction in any medium or format, as long as you give appropriate credit to the original author(s) and the source, provide a link to the Creative Commons licence, and indicate if changes were made. The images or other third party material in this article are included in the article's Creative Commons licence, unless indicated otherwise in a credit line to the material. If material is not included in the article's Creative Commons licence and your intended use is not permitted by statutory regulation or exceeds the permitted use, you will need to obtain permission directly from the copyright holder. To view a copy of this licence, visit http://creativecommons.org/licenses/by/4.0/.

References

1. Liu, Q.; Lan, F.; Zeng, C.; Chen, J.; Wang, J.: A review of proton exchange membrane fuel cell's bipolar plate design and fabrication process. J. Power Sources (2022). https://doi.org/10.1016/j.jpowsour.2022.231543
2. Leng, Y.; Ming, P.; Yang, D.; Zhang, C.: Stainless steel bipolar plates for proton exchange membrane fuel cells: materials, flow channel design and forming process. J. Power Sources (2020). https://doi.org/10.1016/j.jpowsour.2020.227783
3. Vijayakrishnan, M.K.; Palaniswamy, K.; Ramasamy, J.; Kumaresan, T.; Manoharan, K.; Rajagopal, T.K.R.; Maiyalagan, T.; Jothi, V.R.; Yi, S.-C.: Numerical and experimental investigation on 25 cm^2 and 100 cm^2 PEMFC with novel sinuous flow field for effective water removal and enhanced performance. Int. J. Hydrog. Energy (2020). https://doi.org/10.1016/j.ijhydene.2019.05.205
4. Carcadea, E.; Ismail, M.S.; Ingham, D.B.; Patularu, L.; Schitea, D.; Marinoiu, A.; Ion-Ebrasu, D.; Mocanu, D.; Varlam, M.: Effects of geometrical dimensions of flow channels of a large-active-area PEM fuel cel: a CFD study. Int. J. Hydrog. Energy (2021). https://doi.org/10.1016/j.ijhydene.2020.08.150
5. Spernjak, D.; Prasad, A.K.; Advani, S.G.: In situ comparison of water content and dynamics in parallel, single-serpentine, and interdigitated flow fields of polymer electrolyte membrane fuel cells. J. Power Sources (2010). https://doi.org/10.1016/j.jpowsour.2009.12.031
6. Altintas, A.G.; Celik, E.; Karagoz, I.: Investigation of water motion in a fuel cell channel with a reservoir. J. Clean. Prod. (2022). https://doi.org/10.1016/j.jclepro.2022.130975
7. Carcadea, E.; Varlam, M.; Ingham, D.B.; Ismail, M.S.; Patularu, L.; Marinoiu, A.; Schitea, D.: The effect of cathode flow channel size and operating conditions on PEM fuel performance: a CFD modelling study and experimental demonstration. Int. J. Energy Res. (2018). https://doi.org/10.1002/er.4068
8. Zhang, G.; Guan, Z.; Li, D.; Li, G.; Bai, S.; Sun, K.; Cheng, H.: Optimization design of a parallel flow field for PEMFC with bosses in flow channels. Energies (2023). https://doi.org/10.3390/en16145492
9. Li, W.Z.; Yang, W.W.; Zhang, W.Y.; Qu, Z.G.; He, Y.L.: Three-dimensional modeling of a PEMFC with serpentine flow field incorporating the impacts of electrode inhomogeneous compression deformation. Int. J. Hydrog. Energy (2019). https://doi.org/10.1016/j.ijhydene.2019.06.187
10. Çelik, S.; Yagiz, M.; Yildirim, F.; Topcu, A.: Experimental study on the flow field geometry of the PEM fuel cell bipolar plates: the effects of various shaped blocks embedded in serpentine patterm on cell performance. Fuel (2024). https://doi.org/10.1016/j.fuel.2023.130202
11. Choi, K.-S.; Kim, H.-M.; Moon, S.-M.: Numerical studies on the geometrical characterization of serpentine flow-field for efficient PEMFC. Int. J. Hydrog. Energy (2011). https://doi.org/10.1016/j.ijhydene.2010.10.073
12. Valentín-Reyes, J.; León, M.I.; Pérez, T.; Romero-Castañón, T.; Beltrán, J.; Flores-Hernández, J.R.F.; Nava, J.L.: Simulation of an interdigitated flow channel assembled in proton exchange membrane fuel cell (PEMFC). Int. J. Heat Mass Transf. (2022). https://doi.org/10.1016/j.ijheatmasstransfer.2022.123026
13. Guo, N.; Leu, M.; Koylu, U.O.: Network based optimization model for pin-type flow field of polymer electrolyte membrane fuel cell. Int. J. Hydrog. Energy (2013). https://doi.org/10.1016/j.ijhydene.2013.03.066
14. Trogadas, P.; Cho, J.I.S.; Neville, T.P.; Marquis, J.; Wu, B.; Brett, D.J.L.; Coppens, M.-O.: A lung-inspired approach to scalable and robust fuel cell design. Energy Environ. Sci. (2018). https://doi.org/10.1039/C7EE02161E
15. Guo, N.; Leu, M.C.; Koylu, U.O.: Bio-inspired flow field designs for polymer electrolyte membrane fuel cells. Int. J. Hydrog. Energy (2014). https://doi.org/10.1016/j.ijhydene.2014.10.069
16. Damian-Ascencio, C.E.; Saldaña-Robles, A.; Hernandez-Guerrero, A.; Cano-Andrade, S.: Numerical modeling of a proton exchange membrane fuel cell with tree-like flow field channels based on an entropy generation analysis. Energy (2017). https://doi.org/10.1016/j.energy.2017.05.139
17. Abdulla, S.; Patnaikuni, V.S.: Enhanced cross-flow split serpentine flow field design for square cross-sectional polymer electrolyte membrane fuel cell. Electrochim. Acta (2021). https://doi.org/10.1016/j.electacta.2021.138884
18. Hamrang, A.; Abdollahzalah, M.; Bilondi, A.M.; Bagherighajari, F.; Rahgoshay, S.M.; Pascoa, J.C.: Comparison of PEMFC performance with parallel serpentine and parallel serpentine-baffled flow fields under various operating and geometrical conditions; a

parametric study. Int. J. Hydrog. Energy (2023). https://doi.org/10.1016/j.ijhydene.2022.11.122
19. Wu, Y.; Cho, J.I.S.; Neville, T.P.; Meyer, Q.; Ziesche, R.; Boillat, P.; Cochet, M.; Shearing, P.R.; Brett, D.J.L.: Effect of serpentine flow-field design on the water management of polymer electrolyte fuel cells: An in-operando neutron radiography study. J. Power Sources (2018). https://doi.org/10.1016/j.jpowsour.2018.07.085
20. Liu, B.; Huo, W.; Xie, B.; Gao, Q.; Bao, Z.; Li, H.; Wu, K.; He, S.; Du, Q.; Qin, B.; Jiao, K.: Effects of sub-distribution zone structure of bipolar plate on the mass transport of large-area proton exchange membrane fuel cells. Int. J. Heat Mass Transf. (2024). https://doi.org/10.1016/j.ijheatmasstransfer.2024.125169
21. Shateri, M.; Torabi, F.: Influence of liquid water accumulation on the impedence of a PEM fuel cell operating in dead end mode: physical modeling and experimental validation. Electrochim. Acta (2023). https://doi.org/10.1016/j.electacta.2023.141940
22. Benkovic, D.; Fink, C.; Iranzo, A.: Qualitative and quantitative determination of liquid water distribution in a PEM fuel cell. Int. J. Hydrog. Energy (2024). https://doi.org/10.1016/j.ijhydene.2023.09.161
23. Mojica, F.; Rahman, Md.A.; Mora, J.M.; Ocon, J.D.; Chuang, P.-Y.A.: Experimental study of three channel designs with model comparison in a PEM fuel cell. Fuel Cells (2020). https://doi.org/10.1002/fuce.202000002
24. Wang, Y.; Wang, L.; Ji, X.; Zhou, Y.; Wu, M.: Experimental and numerical study of proton exchange membrane fuel cells with a novel compound flow field. ACS Omega (2021). https://doi.org/10.1021/acsomega.1c01924
25. Kaiser, R.; Ahn, C.-Y.; Kim, Y.-H.; Park, J.-C.: Performance and mass transfer evaluation of PEM fuel cells with straight and wavy parallel flow channels of various wavelengths using CFD simulation. Int. J. Hydrog. Energy (2024). https://doi.org/10.1016/j.ijhydene.2023.05.025
26. Boni, M.; Manikanta, Ch.S.; Velisala, V.: Experimental evaluation of proton exchange membrane fuel cell performance with sinusoidal flow channel designs. Int. J. Hydrog. Energy (2024). https://doi.org/10.1016/j.ijhydene.2023.11.340
27. Liu, H.; Li, P.; Juarez-Robles, D.; Wang, K.; Hernandez-Guerrero, A.: Experimental study and comparison of various designs of gas flow fields to PEM fuel cells and cell stack performance. Front. Energy Res. (2014). https://doi.org/10.3389/fenrg.2014.00002
28. Wang, L.; Husar, A.; Zhou, T.; Liu, H.: A parametric study of PEM fuel cell performances. Int. J. Hydrog. Energy (2003). https://doi.org/10.1016/S0360-3199(02)00284-7
29. Sack, J.R.; Urrutia, J.: Handbook of computational geometry. In: Bern, M.; Plassmann, P. (Eds.) Mesh Generation, pp. 291–332. Elsevier, Netherlands (2000)
30. Ngetich, C.C.; Mutua, J.; Kareru, P.; Karanja, K.; Wanjiru, E.: Integrated Taguchi and response surface methods in geometric and parameter optimization of PEM fuel cells. Fuel Cells (2023). https://doi.org/10.1002/fuce.202200209
31. Cai, G.; Liang, Y.; Liu, Z.; Liu, W.: Design and optimization of bio-inspired wave-like channel for a PEM fuel cell applying genetic algorithm. Energy (2020). https://doi.org/10.1016/j.energy.2019.116670
32. Arif, M.; Cheung, S.C.P.; Andrews, J.: Numerical investigation of effects of different flow channel configurations on the 100 cm^2 PEM fuel cell performance under different operating conditions. Catal. Today (2022). https://doi.org/10.1016/j.cattod.2021.07.016
33. Wilberforce, T.; El-Hassan, Z.; Khatib, F.N.; Makky, A.A.; Mooney, J.; Barouaji, A.; Carton, J.G.; Olabi, A.-G.: Development of bi-polar plate design of PEM fuel cell using CFD techniques. Int. J. Hydrog. Energy (2017). https://doi.org/10.1016/j.ijhydene.2017.08.093
34. Limjeerajarus, N.; Charoen-amornkitt, P.: Effect of different flow field designs and number of channels on performance of a small PEFC. Int. J. Hydrog. Energy (2015). https://doi.org/10.1016/j.ijhydene.2015.04.007
35. Kupeli, S.; Celik, E.; Karagoz, I.: Response of a proton exchange membrane fuel cell to step changes in mass flow rates. Fuel Cells. (2021). https://doi.org/10.1002/fuce.202000170
36. Su, A.; Weng, F.-B.; Hsu, C.-Y.; Chen, Y.-M.: Studies on flooding in PEM fuel cell cathode channels. Int. J. Hydrog. Energy (2006). https://doi.org/10.1016/j.ijhydene.2005.12.019
37. Li, Y.; Bi, J.; Tang, M.; Lu, G.: Snowflake bionic flow channel design to optimize the pressure drop and flow uniform of proton exchange membrane fuel cells. Micromachines (2022). https://doi.org/10.3390/mi13050665
38. Shimpalee, S.; Greenway, S.; Van Zee, J.W.: The impact of channel path length on PEMFC flow-field design. J. Power Sources (2006). https://doi.org/10.1016/j.jpowsour.2006.01.099